

# Noise Correlation in Compact Diversity Receivers

Carlo P. Domizioli, Brian L. Hughes, Kevin G. Gard, and Gianluca Lazzi

**Abstract**—The impact of antenna mutual coupling on signal correlation in multi-antenna receivers has been studied in great detail. By contrast, there has been little work on how mutual coupling affects noise. In this paper we present a noise model for a diversity receiver that includes noise generated by the antennas, front-end amplifiers, and other receiver components. This model shows that noise in a compact diversity receiver may be spatially correlated. Expressions relating noise correlation to properties of the antennas and amplifiers are derived and its impact on the outage probability of an optimal diversity combiner is studied. Examples illustrating the relationship between mutual coupling and noise correlation demonstrate how different noise sources may impact performance in profoundly different ways.

**Index Terms**—Antenna arrays, mutual coupling, noise, receivers, diversity methods.

## I. INTRODUCTION

RECEIVE diversity systems that employ multiple antennas provide an effective and bandwidth-efficient means of reducing the impact of multipath fading. Performance benefits associated with diversity are dependent on the correlation between the fading path gains in each diversity branch, with independence between the branches being ideal. However, this typically requires antenna separations of several wavelengths – a constraint that is often impractical for compact mobile receivers. Furthermore, at close spacings the antennas may become strongly coupled, which may further correlate the signals. These issues were initially considered in [1], and have also received attention within other fields of interest such as adaptive arrays [2] and more recently in multiple-input, multiple-output (MIMO) systems [3] - [8].

While the above studies have carefully modeled the impact of coupling on the signal component, relatively little attention has been paid to noise. In fact, most of the works cited above do not include detailed models of noise. Instead, noise is modeled as spatially white and Gaussian, regardless of its source or the receiver design. However, real receivers are plagued by diverse noise sources. These sources are affected by antenna coupling, matching networks and amplifiers in different ways. Since the signal and noise play equal roles in determining most system performance metrics, a channel model that does not correctly represent noise cannot be expected to correctly predict performance.

Paper approved by G. K. Karagiannidis, the Editor for Fading Channels and Diversity of the IEEE Communications Society. Manuscript received November 14, 2008; revised June 19, 2009.

The authors are with the Department of Electrical and Computer Engineering, North Carolina State University, Raleigh, NC 27695-7914 (e-mail: {cpdomizi, blhughes, kevin\_gard, lazzi}@ncsu.edu).

This material is based upon work supported by the National Science Foundation under grant CCF-0728803. Portions of this paper were presented at the 2007 IEEE Global Communications Conference.

Digital Object Identifier 10.1109/TCOMM.2010.080601

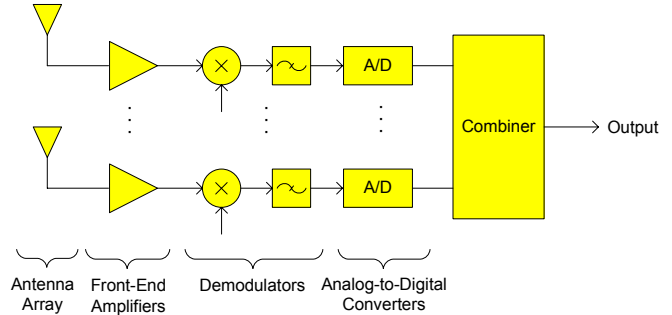


Fig. 1. Basic diagram of a post-detection diversity receiver.

In this paper we evaluate the performance of an optimal diversity combiner in the presence of antenna mutual coupling and various receiver noise sources. Our receiver noise model is divided into three components: the antennas, front-end amplifiers, and everything else “downstream” from the amplifiers. This approach will allow us to characterize the unique properties of each source of noise, and to determine how each is impacted by antenna mutual coupling. Prior approaches have only modeled noise from either the antennas [10],[12] or amplifiers [9],[11], and a detailed study of how mutual coupling and the receiver structure affect noise correlation is lacking. For example, both [9] and [11] present results for specific amplifiers, but there is little discussion of how certain parameters of the amplifier (e.g., unilaterality, gain, noise figure) affect noise correlation and performance. It is the goal of this paper to clearly articulate the characteristics of each receiver noise source and study their impact on optimal diversity performance.

We begin with an overview of our receiver model, which was originally introduced in some preliminary work [13]. In order to orient the reader to receiver noise modeling we have included a discussion of typical noise budgets for a single-antenna receiver. This analysis suggests that for many receivers no single source of noise is dominant. Using this model we find an expression for the signal collected by the combiner, and formulas for the outage probability of an optimal combiner are derived. In contrast to [9] and [11] (which use scattering and transmission parameters, respectively), we use an impedance formulation to describe the receiver, for which the familiar concepts of voltage and current may be more accessible to the reader unfamiliar with microwave circuit analysis. In the subsequent section we attempt to connect our model with the typical i.i.d. noise assumption. It is shown that in the presence of coupled antennas, strong assumptions on both the receiver structure and dominant source of noise may be needed to justify the white noise model. After introducing

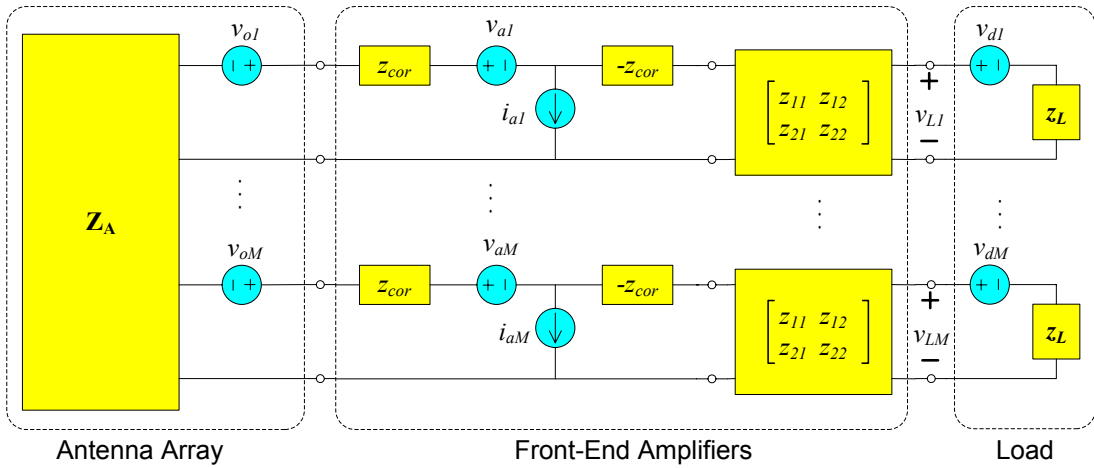


Fig. 2. Circuit model of a post-detection diversity receiver.

matching networks into our model, numerical results are presented. Several scenarios of interest are presented, including a detailed study of receiver noise correlation, a parametric sweep of various receiver parameters and noise sources, and the impact of directional fading and sky noise. From these results and the developed theory we conclude that noise correlation in compact diversity receivers depends on the interaction between the dominant sources of noise and the coupled antennas – a result that may have profound implications for the selection of receiver components. For example, in uncoupled systems only the total noise power generated by a front-end amplifier is of interest, while in the presence of coupled antennas one should be concerned with how the noise is distributed between the input and output ports.

## II. RECEIVER MODEL

A typical post-detection diversity receiver is illustrated in Fig. 1. The signals collected by each antenna are amplified and demodulated prior to A/D conversion and diversity combining. We assume coupling occurs only between antennas; there is no coupling between the amplifiers, demodulators or A/D converters in each branch. We further assume a narrowband system, so all impedances are constant over the system bandwidth and all signals can be expressed in complex baseband form. A circuit model of this  $M$ -branch receiver is illustrated in Fig. 2. Both the antenna array and front-end amplifiers are represented by equivalent noisy circuit models. As will be seen later, noise generated by receiver components “downstream” from the front-end amplifiers is considerably less affected by antenna coupling, so we shall lump them together as a “load” on the amplifiers. Below we discuss these circuit models in more detail.

### A. Antenna Array

The function of an antenna is to convert an incident electromagnetic field into a voltage across the antenna terminals. When the antennas of an array are closely spaced, the terminal voltage of each antenna depends not only on the field at that antenna but also on the currents flowing through neighboring antennas. The relationship between the terminal voltages and

currents, arranged in  $M$ -dimensional column vectors  $\mathbf{v}$  and  $\mathbf{i}$ , respectively, can be modeled as

$$\mathbf{v} = \mathbf{Z}_A \mathbf{i} + \mathbf{v}_o, \quad (1)$$

where  $\mathbf{Z}_A$  is an  $M \times M$  impedance matrix and  $\mathbf{v}_o$  is an  $M$ -dimensional vector of open-circuit (induced) voltages. Here  $[\mathbf{Z}_A]_{nn}$  is the *self-impedance* of antenna  $n$ , and  $[\mathbf{Z}_A]_{nm}$  is the *mutual impedance* between antennas  $n$  and  $m$ . Approximate formulas for these impedances are available for thin dipoles [14, ch. 8]; other types of antennas may be evaluated by numerical techniques.

We assume a frequency-flat, Rayleigh fading environment, so

$$\mathbf{v}_o = \mathbf{h}x + \mathbf{n}_o, \quad (2)$$

where  $x$  is the transmitted symbol,  $\mathbf{h}$  is a vector of fading path gains, and  $\mathbf{n}_o$  is noise. The symbol energy is  $\mathcal{E} \triangleq E[|x|^2]$ , where  $E[\cdot]$  denotes the expectation. For Rayleigh fading  $\mathbf{h}$  has a zero-mean, circularly-symmetric, complex Gaussian distribution, denoted by  $\mathbf{h} \sim \mathcal{CN}(\mathbf{0}, \Sigma_{\mathbf{h}})$ , where  $\Sigma_{\mathbf{h}} = E[\mathbf{h}\mathbf{h}^\dagger]$  is the fading correlation matrix.

For perfectly conducting antennas,  $\mathbf{n}_o$  is the voltage induced in the array by noise sources in the surrounding environment. These sources may include thermal radiation, cosmic background, and interference from other electronic devices. We will use the classical model for spherically isotropic thermal radiation in which the array is surrounded by a blackbody enclosure at temperature  $T_A$  K (cf., [15, Ch. 6]). The noise voltage is then [16]  $\mathbf{n}_o \sim \mathcal{CN}(\mathbf{0}, 4kT_A B \mathbf{R}_A)$ , where  $\mathbf{R}_A \triangleq \frac{1}{2}(\mathbf{Z}_A + \mathbf{Z}_A^\dagger)$ ,  $\dagger$  denotes the conjugate-transpose,  $k = 1.38 \times 10^{-23}$  J/K is Boltzmann’s constant and  $B$  is the bandwidth in Hz. Gaussian interference may be modeled by a simple generalization of this model that accounts for its spatial distribution (the above model is *isotropic*) [17, pg. 642]; an example will be provided in Sec. VII-F. Note that if the array is imbedded in a linear medium, the reciprocity theorem of electromagnetics [14, pg. 144] implies  $\mathbf{Z}_A$  is symmetric, and so  $\mathbf{R}_A = \text{Re}[\mathbf{Z}_A]$ .

### B. Front-End Amplifiers

An amplifier is usually well-modeled within its dynamic range as a linear, noisy two-port network, so it can be

represented by a Thevenin equivalent network with impedance matrix

$$\begin{bmatrix} z_{11} & z_{12} \\ z_{21} & z_{22} \end{bmatrix} \quad (3)$$

and open-circuit noise voltages  $n_1$  and  $n_2$  at the input and output ports, respectively. Many noise sources, such as thermal and shot noise, are well-modeled [15, pg. 42] as  $n_i \sim \mathcal{CN}(0, \sigma_i^2)$ , with  $\rho_{12} \triangleq \frac{\mathbb{E}[n_1 n_2^*]}{\sigma_1 \sigma_2} \neq 0$  in general. Thus amplifier noise may be characterized by the *noise parameters*  $\{\sigma_1, \sigma_2, \rho_{12}\}$ . However, these particular parameters are rarely used in practice. Below we briefly present some of the more common noise metrics relevant to this paper.

The Rothe-Dahlke [18] noise model, shown for each amplifier in Fig. 2, is typically used to model amplifiers instead of the Thevenin equivalent model discussed above. The voltage and current sources at the input port, denoted by  $v_a$  and  $i_a$ , are related to the parameters above by

$$v_a = n_1 + \frac{z_{\text{cor}} - z_{11}}{z_{21}} n_2, \quad i_a = -\frac{n_2}{z_{21}} \quad (4)$$

where  $z_{\text{cor}} = r_{\text{cor}} + jx_{\text{cor}} = z_{11} - z_{21}\rho_{12}\frac{\sigma_1}{\sigma_2}$  is the *correlation impedance* defined so that  $\mathbb{E}[v_a i_a^*] = 0$ . A common convention is to normalize the variances of these noise sources by the thermal noise power generated by a  $1 \Omega$  resistor at standard temperature  $T_0 = 290 \text{ K}$ . Thus, the *equivalent noise resistance* of the voltage source and the *equivalent noise conductance* of the current source are given by

$$r_a = \frac{\mathbb{E}[|v_a|^2]}{4kT_0B}, \quad g_a = \frac{\mathbb{E}[|i_a|^2]}{4kT_0B}. \quad (5)$$

The amplifiers in Fig. 2 are identical and uncoupled, so the joint distributions of the  $M$  amplifier voltage and current sources are  $\mathbf{v}_a \sim \mathcal{CN}(\mathbf{0}, 4kT_0B r_a \mathbf{I})$  and  $\mathbf{i}_a \sim \mathcal{CN}(\mathbf{0}, 4kT_0B g_a \mathbf{I})$ , where  $\mathbf{I}$  is the identity matrix.

An important amplifier noise metric is the *noise factor*,  $F_{\text{amp}}$ , defined as the ratio of the output noise power to the noise power contributed by a source alone, when a source impedance  $z_s = r_s + jx_s$  at standard temperature is connected to the input port, i.e., [18]

$$F_{\text{amp}} = 1 + \frac{1}{r_s} \left( r_a + g_a |z_s + z_{\text{cor}}|^2 \right). \quad (6)$$

The noise factor is useful because it relates the input and output signal-to-noise ratios (SNRs) of the amplifier, given in dB by  $\text{SNR}_{\text{out}} = \text{SNR}_{\text{in}} - \text{NF}$ , where  $\text{NF} = 10 \log_{10} F_{\text{amp}}$  is the *noise figure*. Note that  $F_{\text{amp}}$  attains its minimum value  $F_{\text{min}}$  when  $z_s = z_{\text{opt}}$  where [18]

$$F_{\text{min}} = 1 + 2 \left( g_a r_{\text{cor}} + \sqrt{g_a r_a + (g_a r_{\text{cor}})^2} \right) \quad (7)$$

$$z_{\text{opt}} = \sqrt{r_a/g_a + r_{\text{cor}}^2} - jx_{\text{cor}}. \quad (8)$$

Note the parameters  $\{F_{\text{min}}, g_a, z_{\text{opt}}\}$  are typically used to characterize the noise statistics of low-noise amplifiers (LNAs),<sup>1</sup> and are related to the noise factor by

$$F_{\text{amp}} = F_{\text{min}} + \frac{g_a}{r_s} |z_s - z_{\text{opt}}|^2. \quad (9)$$

<sup>1</sup>A variation of these parameters based on the admittance version of the Rothe-Dahlke model are  $\{F_{\text{min}}, R_a, Y_{\text{opt}}\}$ . For microwave amplifiers a reflection coefficient  $\Gamma_{\text{opt}}$  is usually given in place of  $Y_{\text{opt}}$  [17, pg. 558].

### C. Load

Since the receiver chains downstream from the amplifiers in Fig. 1 are assumed to be electrically isolated, the noise in each branch is independent and the impedances are uncoupled. Each branch consists of filters, mixers and other analog devices that generate noise. Here we reference all downstream noise to the amplifier output and assume that each branch may be modeled by an impedance  $z_L$  and a zero-mean Gaussian noise voltage  $v_{di}$  with equivalent noise resistance  $r_d$ , as shown in Fig. 2. We denote the noise factor of the downstream components by  $F_{\text{dow}}$ .

## III. NOISE IN SINGLE-ANTENNA RECEIVERS

Prior studies of noise in multi-antenna receivers have assumed either antenna [10] or amplifier [9],[11] noise is dominant, and downstream noise is usually neglected. In this section we examine this assumption by considering typical noise budgets for a *single-antenna* receiver, which suggest that one may not always be able to identify a single dominant source of noise. The results of this section may be inferred from any text on receiver design (e.g., [17, Ch. 10-13]).

Consider the model of Fig. 2 with  $M = 1$ . As discussed in Sec. II-B, for  $T_A = T_0$  the SNR drop across the receiver is equal to its noise factor  $F_{\text{Rx}}$ . For  $T_A \neq T_0$ , it can be shown (cf., [17, pg. 641]) that the SNR drop across the receiver is  $1 + \frac{T_0}{T_A}(F_{\text{Rx}} - 1)$ , so the SNR at the load is

$$\sigma = \frac{\mathcal{E}}{4kT_0B r_A} \cdot \frac{1}{\frac{T_A}{T_0} + F_{\text{Rx}} - 1}. \quad (10)$$

If  $G_{\text{amp}} = |z_{21}/(z_A + z_{11})|^2$  is the amplifier gain, then the receiver noise factor is related to the amplifier and downstream noise factors by (cf., [17, pg. 495])

$$F_{\text{Rx}} = F_{\text{amp}} + \frac{F_{\text{dow}} - 1}{G_{\text{amp}}}. \quad (11)$$

We may now use (10) and (11) to make the following assertions for single-antenna receivers:

- Assuming typical receiver noise figures of 3 – 10 dB, in order for antenna noise to dominate we would need  $T_A$  to be at least 10 – 100 times larger than the standard temperature.
- On the other hand, antenna noise of purely thermal origin typically results in  $T_A/T_0 \in [-3, 0] \text{ dB}$  [17, Fig. 13.6], so receiver noise figures of at least 7 – 10 dB would be required in order to neglect thermal antenna noise.
- Many microwave amplifiers have  $F_{\text{amp}} G_{\text{amp}} \in [10, 20] \text{ dB}$  [17, Tbl. 10.2], in which case the downstream noise figure<sup>2</sup> may need to be as low as 1 – 10 dB to be considered negligible.

From this discussion we conclude that one must typically include all three noise sources. As an example, consider the receiver in [17, Ex. 10.2]. The antenna temperature is 150 K, the LNA has a 2 dB noise figure and 10 dB gain, and the downstream components consist of a filter with 1 dB loss and

<sup>2</sup>In contrast to the LNA, some downstream components are lossy, noisy devices such as filters and mixers, so noise figures in the 5 – 10 dB range are not uncommon.

a mixer with 4 dB noise figure. Here no noise source can be neglected since

$$\frac{T_A}{T_0} = 0.517, \quad F_{\text{amp}} - 1 = 0.585, \quad \frac{F_{\text{dow}} - 1}{G_{\text{amp}}} = 0.216.$$

#### IV. OUTAGE PROBABILITY OF AN OPTIMAL COMBINER

We now derive the outage probability of an optimal diversity combiner for the system in Fig. 2. We begin by finding an expression for the voltage across the load,  $\mathbf{v}_L$ , and then use this expression to determine the optimal combiner. We assume throughout that all impedance matrices are invertible, so every non-zero current vector input produces a non-zero voltage vector.

The  $M$  uncoupled amplifiers may be collectively viewed as a  $2M$ -port network with input and output open-circuit voltages  $\mathbf{v}_a + (z_{\text{cor}} - z_{11})\mathbf{i}_a$  and  $-z_{21}\mathbf{i}_a$ , respectively, and impedance matrix

$$\begin{bmatrix} z_{11}\mathbf{I} & z_{12}\mathbf{I} \\ z_{21}\mathbf{I} & z_{22}\mathbf{I} \end{bmatrix}, \quad (12)$$

where each  $\mathbf{I}$  is  $M \times M$ . Relating the voltages and currents at the input and output of this network to those of the antenna array, we can show that the antenna array plus amplifiers comprise an  $M$ -port network with open-circuit voltage  $\mathbf{u}$  and impedance matrix  $\mathbf{Z}$ , where

$$\begin{aligned} \mathbf{u} &= \mathbf{C}(\mathbf{v}_o - \mathbf{v}_a) - [(z_{\text{cor}} - z_{11})\mathbf{C} + z_{21}\mathbf{I}]\mathbf{i}_a \\ \mathbf{Z} &= -z_{12}\mathbf{C} + z_{22}\mathbf{I}, \end{aligned} \quad (13)$$

and  $\mathbf{C} = z_{21}(\mathbf{Z}_A + z_{11}\mathbf{I})^{-1}$ . By voltage division between this network and the load, we obtain

$$\begin{aligned} \mathbf{v}_L &= z_L(\mathbf{Z} + z_L\mathbf{I})^{-1}\mathbf{u} + \mathbf{Z}(\mathbf{Z} + z_L\mathbf{I})^{-1}\mathbf{v}_d \\ &= \mathbf{G}[\mathbf{v}_o - \mathbf{v}_a - (\mathbf{Z}_A + z_{\text{cor}}\mathbf{I})\mathbf{i}_a + \mathbf{K}\mathbf{v}_d], \end{aligned} \quad (14)$$

where

$$\mathbf{G} = \frac{z_{21}z_L}{z_L + z_{22}} \left( \mathbf{Z}_A + \frac{z_{11}(z_L + z_{22}) - z_{12}z_{21}}{z_L + z_{22}} \mathbf{I} \right)^{-1} \quad (15)$$

$$\mathbf{K} = \frac{z_{22}}{z_{21}z_L} \left( \mathbf{Z}_A + \frac{z_{11}z_{22} - z_{12}z_{21}}{z_{22}} \mathbf{I} \right). \quad (16)$$

Since we have assumed  $\mathbf{G}$  is invertible, finding an optimal combiner for  $\mathbf{v}_L$  is equivalent to finding one for  $\mathbf{G}^{-1}\mathbf{v}_L$ . Since the latter expression is simpler, we take the observed signal to be

$$\mathbf{r} \triangleq \mathbf{G}^{-1}\mathbf{v}_L = \mathbf{h}x + \mathbf{n}, \quad (17)$$

where the second equality follows by substituting (2) into (14), and defining the noise as

$$\mathbf{n} \triangleq \mathbf{n}_o - \mathbf{v}_a - (\mathbf{Z}_A + z_{\text{cor}}\mathbf{I})\mathbf{i}_a + \mathbf{K}\mathbf{v}_d. \quad (18)$$

Finally, recalling that  $\mathbf{n}_o \sim \mathcal{CN}(\mathbf{0}, 4kT_A B \mathbf{R}_A)$ ,  $\mathbf{v}_a \sim \mathcal{CN}(\mathbf{0}, 4kT_0 B r_a \mathbf{I})$ ,  $\mathbf{i}_a \sim \mathcal{CN}(\mathbf{0}, 4kT_0 B g_a \mathbf{I})$  and  $\mathbf{v}_d \sim \mathcal{CN}(\mathbf{0}, 4kT_0 B r_d \mathbf{I})$  are mutually independent, we obtain  $\mathbf{n} \sim \mathcal{CN}(\mathbf{0}, \mathbf{\Sigma}_n)$  where

$$\begin{aligned} \mathbf{\Sigma}_n &= 4kT_0 B \left[ \frac{T_A}{T_0} \mathbf{R}_A + r_a \mathbf{I} \right. \\ &\quad \left. + g_a (\mathbf{Z}_A + z_{\text{cor}}\mathbf{I}) (\mathbf{Z}_A + z_{\text{cor}}\mathbf{I})^\dagger + r_d \mathbf{K}\mathbf{K}^\dagger \right] \end{aligned} \quad (19)$$

We now derive the optimal linear combiner for the observation (17). For a combiner of the form  $y = \mathbf{w}^\dagger \mathbf{r}$ , the *instantaneous SNR* at the combiner output is

$$\gamma(\mathbf{w}) = \mathcal{E} \frac{|\mathbf{w}^\dagger \mathbf{h}|^2}{\mathcal{E} |\mathbf{w}^\dagger \mathbf{n}|^2} = \mathcal{E} \frac{\mathbf{w}^\dagger \mathbf{h} \mathbf{h}^\dagger \mathbf{w}}{\mathbf{w}^\dagger \mathbf{\Sigma}_n \mathbf{w}}. \quad (20)$$

For i.i.d. noise (e.g.,  $\mathbf{\Sigma}_n = \mathbf{I}$ ) it is well-known [19] that the maximum-ratio combiner (MRC)  $\mathbf{w} \propto \mathbf{h}$  uniquely maximizes  $\gamma(\mathbf{w})$ . It is a simple exercise [13] to show that  $\mathbf{w} \propto \mathbf{\Sigma}_n^{-1} \mathbf{h}$  maximizes (20) for any noise correlation. The resulting optimal SNR is

$$\gamma^\circ = \max_{\mathbf{w}} \gamma(\mathbf{w}) = \mathcal{E} \cdot \mathbf{h}^\dagger \mathbf{\Sigma}_n^{-1} \mathbf{h}. \quad (21)$$

The performance of receive diversity systems is often measured by the outage probability, defined as  $P_{\text{out}}(\tau) = \Pr\{\gamma^\circ \leq \tau\}$ , where  $\tau$  is a non-negative threshold. A closed-form expression for the outage can be obtained using the results of [1]: If  $0 < \lambda_1 < \dots < \lambda_M$  are the distinct eigenvalues of the *SNR matrix*

$$\mathbf{\Sigma} \triangleq \mathcal{E} \cdot \mathbf{\Sigma}_h^{1/2} \mathbf{\Sigma}_n^{-1} \mathbf{\Sigma}_h^{1/2}, \quad (22)$$

and  $\mathbf{A}^{1/2}$  is the positive-definite square root of a positive definite matrix  $\mathbf{A}$  [20, pg. 406], then<sup>3</sup>

$$P_{\text{out}}(\tau) = \sum_{j=1}^M \frac{\lambda_j^{M-1} (1 - e^{-\tau/\lambda_j})}{\prod_{i \neq j} (\lambda_j - \lambda_i)}. \quad (23)$$

The restriction of distinct eigenvalues on  $\mathbf{\Sigma}$  includes a large class of  $\mathbf{\Sigma}_h$  and  $\mathbf{\Sigma}_n$ ; however, an important exception occurs when  $\mathbf{\Sigma}_h$  and  $\mathbf{\Sigma}_n$  are proportional. One example of proportional  $\mathbf{\Sigma}_h$  and  $\mathbf{\Sigma}_n$  occurs when both the fading and noise are i.i.d.; a second example will be presented in Section VII-D. In this case, the SNR matrix (22) reduces to  $\mathbf{\Sigma} = \sigma \mathbf{I}$ , where  $\sigma$  is the single-antenna SNR (10), and we may use Brennan's outage formula [19]:

$$P_{\text{out}}(\tau) = \frac{1}{(M-1)!} \int_0^{\tau/\sigma} t^{M-1} e^{-t} dt. \quad (24)$$

#### V. SPATIALLY WHITE NOISE

Most prior studies of receive diversity assume spatially white noise. In this section we examine some sufficient conditions for uncorrelated noise in our model. The total noise voltage across the load is  $\mathbf{G}\mathbf{n}$ , where  $\mathbf{G}$  and  $\mathbf{n}$  are defined in (15) and (18). Thus the correlation matrices of noise contributions from the antennas, amplifiers, and downstream components are given by

$$\mathbf{\Sigma}_{\text{ant}} = 4kT_A B \mathbf{G} \mathbf{R}_A \mathbf{G}^\dagger \quad (25)$$

$$\begin{aligned} \mathbf{\Sigma}_{\text{amp}} &= 4kT_0 B \mathbf{G} \left[ r_a \mathbf{I} \right. \\ &\quad \left. + g_a (\mathbf{Z}_A + z_{\text{cor}}\mathbf{I}) (\mathbf{Z}_A + z_{\text{cor}}\mathbf{I})^\dagger \right] \mathbf{G}^\dagger \end{aligned} \quad (26)$$

$$\mathbf{\Sigma}_{\text{dow}} = \frac{4kT_0 B r_d}{|z_L + z_{22}|^2} (z_{22}\mathbf{I} - z_{12}\mathbf{G})(z_{22}\mathbf{I} - z_{12}\mathbf{G})^\dagger \quad (27)$$

When the antennas are uncoupled,  $\mathbf{Z}_A$  is diagonal and from (15) we see that each of the above correlation matrices is

<sup>3</sup>This follows from the Appendix of [1] by writing  $\gamma^\circ = \mathbf{h}_w^\dagger \mathbf{\Sigma} \mathbf{h}_w$ , where  $\mathbf{h}_w \sim \mathcal{CN}(\mathbf{0}, \mathbf{I})$ .

diagonal, and so the noise is spatially white. Not surprisingly, mutual coupling is therefore necessary in our model for the noise to be correlated. It is not, however, sufficient: the noise can be white when the antennas are coupled. Since the amplifier and downstream noise sources are independent, isolating these sources from the coupled antennas should result in spatially white noise. Two examples of this are given below.

An amplifier that provides zero gain from its output to input port (the reverse signal path) is said to be *unilateral* [17, pg. 524]. This condition implies  $z_{12} = 0$  in Fig. 2 and results in a diagonal  $\Sigma_{\text{dow}}$  in (27). Since most practical front-end amplifiers are approximately unilateral ( $z_{12} \approx 0$ ), we expect that a spatially white noise model is justified if there is a dominant source of noise downstream from the amplifiers. Later we will illustrate this result for a specific LNA.

Other assumptions may also result in white noise. In [11] the dominant noise sources are assumed to be unilateral front-end amplifiers with the property that the total noise current at the amplifier output is independent of the source impedance. To see the implications of this assumption, observe that when an impedance  $z_s$  is connected to the input port of the Rothe-Dahlke amplifier model (cf. Sec II-B) with  $z_{12} = 0$ , the noise current at the output is

$$i_{\text{out}} = \frac{z_{21}}{(z_{11} + z_s)(z_{22} + z_L)} [v_a + (z_{\text{cor}} + z_s) i_a]. \quad (28)$$

This expression is independent of  $z_s$  only if  $v_a = i_a(z_{11} - z_{\text{cor}})$ . From (4), this is equivalent to assuming that the input port is noise free,  $n_1 = 0$ , which implies  $r_a = 0$  and  $z_{\text{cor}} = z_{11}$ . It is easy to show that these conditions, together with the assumption  $z_{12} = 0$ , do indeed imply that  $\Sigma_{\text{amp}}$  in (26) is diagonal, as asserted in [11]. However, it appears that many practical amplifiers (e.g., [24]) do not satisfy these conditions, and so the amplifier noise may be correlated.

These observations suggest that, when the antennas are coupled, strong assumptions on the front-end amplifiers and downstream components may be needed to justify a white noise model. Even when the noise sources in each branch are independent (e.g., amplifier noise), these sources can interact through the coupled antennas to produce correlated noise in the observed signal. White noise can arise when the amplifiers completely isolate these sources from the antennas, but many amplifiers do not satisfy the conditions needed for this to occur.

## VI. MATCHING NETWORKS

The transfer of signal and noise power between two networks may be controlled using impedance matching techniques (cf., [17, Ch. 5]). Ideally a matching network is formed with passive, reactive elements so it is noiseless, lossless, and reciprocal. Consider a  $2M$ -port matching network inserted between the antennas and front-end amplifiers in Fig. 2 with impedance matrix

$$\begin{bmatrix} \mathbf{Z}_{M11} & \mathbf{Z}_{M12} \\ \mathbf{Z}_{M21} & \mathbf{Z}_{M22} \end{bmatrix} \quad (29)$$

If  $\mathbf{v}_1, \mathbf{v}_2$  and  $\mathbf{i}_1, \mathbf{i}_2$  denote the voltages and currents at the input and output of the network, respectively, the matrices in

(29) are defined by the circuit equations

$$\begin{aligned} \mathbf{v}_1 &= \mathbf{Z}_{M11} \mathbf{i}_1 + \mathbf{Z}_{M12} \mathbf{i}_2 \\ \mathbf{v}_2 &= \mathbf{Z}_{M21} \mathbf{i}_1 + \mathbf{Z}_{M22} \mathbf{i}_2, \end{aligned} \quad (30)$$

where each  $\mathbf{Z}_{Mnm}$  is an  $M \times M$  matrix. The network is lossless (no power is dissipated within it) provided the following conditions are satisfied [21, pg. 13]:  $\mathbf{Z}_{M11} = -\mathbf{Z}_{M11}^\dagger$ ,  $\mathbf{Z}_{M22} = -\mathbf{Z}_{M22}^\dagger$ ,  $\mathbf{Z}_{M21} = -\mathbf{Z}_{M12}^\dagger$ . Most passive networks are also reciprocal, in which case  $\mathbf{Z}_{M11} = \mathbf{Z}_{M11}^T$ ,  $\mathbf{Z}_{M22} = \mathbf{Z}_{M22}^T$ , and  $\mathbf{Z}_{M21} = \mathbf{Z}_{M12}^T$ , where the  $T$  superscript denotes transpose.

From the standpoint of the rest of the receiver, the antennas plus matching comprise a noisy linear network which can be represented by a Thevenin equivalent circuit with [21]

$$\mathbf{v}'_o = \mathbf{M} \mathbf{v}_o, \quad \mathbf{Z}'_A = -\mathbf{M} \mathbf{Z}_{M12} + \mathbf{Z}_{M22}, \quad (31)$$

where  $\mathbf{M} = \mathbf{Z}_{M21} (\mathbf{Z}_A + \mathbf{Z}_{M11})^{-1}$ . Thus the results of Section IV still apply with  $\Sigma_{\text{h}}$  replaced by  $\mathbf{M} \Sigma_{\text{h}} \mathbf{M}^\dagger$  and  $\mathbf{Z}_A$  replaced by  $\mathbf{Z}'_A$ . In particular, the SNR matrix (22) becomes<sup>4</sup>

$$\Sigma = \frac{\mathcal{E}}{4kT_0B} \mathbf{M} \Sigma_{\text{h}} \mathbf{M}^\dagger \left[ \frac{T_A}{T_0} \mathbf{R}'_A + r_a \mathbf{I} + g_a (\mathbf{Z}'_A + z_{\text{cor}} \mathbf{I}) (\mathbf{Z}'_A + z_{\text{cor}} \mathbf{I})^\dagger + r_d \mathbf{K}' \mathbf{K}'^\dagger \right]^{-1}, \quad (32)$$

where  $\mathbf{R}'_A \triangleq \frac{1}{2} (\mathbf{Z}'_A + \mathbf{Z}'_A{}^\dagger)$  and  $\mathbf{K}'$  is given by (16) with  $\mathbf{Z}_A$  replaced by  $\mathbf{Z}'_A$ .

## VII. NUMERICAL RESULTS

We now present numerical results for several examples of our model. In each case we use (23) and (32) to calculate the diversity gain at 1% outage for  $M = 2, 4$  antennas, where diversity gain is defined as the difference in SNR between a given outage curve and the  $M = 1$  curve at a fixed probability. We begin with a description of the parameters<sup>5</sup> common to each example.

### A. System Parameters

We consider a uniform linear array (ULA) of half-wavelength dipoles with inter-element spacings  $0.01\lambda \leq d \leq \lambda$ , where  $\lambda$  is the wavelength. The received electric field is composed of a large number (in the sense of the central limit theorem for Rayleigh fading) of plane waves with independent and uniformly-distributed polarization angles<sup>6</sup> and phases. In a spherical coordinate system with  $\theta$  and  $\phi$  denoting the zenith and azimuth, respectively, let  $p(\theta, \phi) \sin \theta d\theta d\phi$  denote the probability that a plane wave arrives within solid angle

<sup>4</sup>For convenience we have expressed the SNR matrix as  $\mathcal{E} \cdot \Sigma_{\text{h}} \Sigma_{\text{n}}^{-1}$ , which has the same eigenvalues (and therefore results in the same outage probability) as the SNR matrix defined in (22).

<sup>5</sup>Since diversity gain is unchanged for scalar multiples of the fading and noise correlation matrices such as  $\mathcal{E}$  and  $B$ , values for these parameters are not provided.

<sup>6</sup>Since dipoles respond only to the field component parallel to its axis, we may equivalently consider co-polarized waves with i.i.d. amplitudes  $\alpha \in (0, 1)$ , where  $\Pr[\alpha \leq x] = 1 - \frac{2}{\pi} \cos^{-1} x$ . Regardless, the average power loss resulting from random amplitudes may be absorbed into the signal energy  $\mathcal{E}$ .

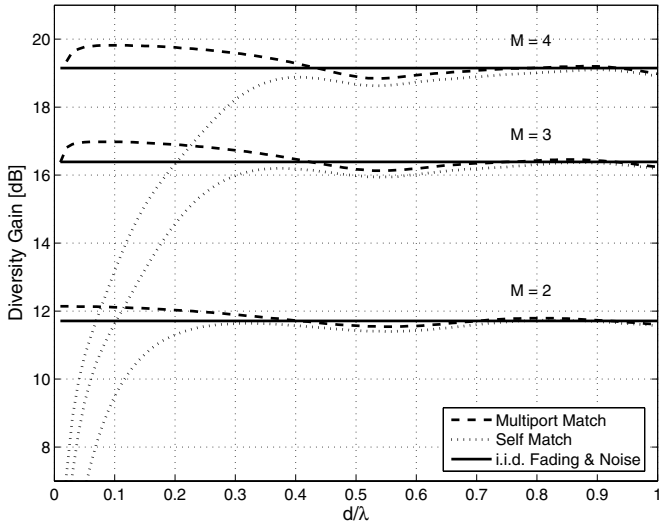


Fig. 3. Diversity gain at 1% outage for multiport and self matching.

$\sin \theta d\theta d\phi$ . Then the entries  $[\Sigma_{\mathbf{h}}]_{nm}$  of the fading correlation matrix are given by (cf., [22])

$$\int_0^{2\pi} \int_0^\pi g_n(\theta, \phi) g_m^*(\theta, \phi) e^{j \frac{2\pi}{\lambda} d(m-n) \sin \theta \cos \phi} p(\theta, \phi) \sin \theta d\theta d\phi \quad (33)$$

where the antenna pattern  $g_n(\theta, \phi)$  is defined as the voltage induced in the  $n^{\text{th}}$  dipole by a zero-phase, unit-amplitude,  $\theta$ -polarized plane wave with angle-of-arrival (AoA)  $(\theta, \phi)$ . In the first few examples we shall consider the standard 2D scattering model  $p(\theta, \phi) = \frac{1}{2\pi} \delta(\theta - \frac{\pi}{2})$ . We shall initially take  $T_A = T_0$ , and consider the impact of antenna temperature in a later example.

Approximate expressions for the impedance matrix  $\mathbf{Z}_A$  and antenna patterns  $g_n(\theta, \phi)$  are given in [14, Ch. 8] for infinitesimally thin wire dipoles. To account for scattering among the antennas, however, we evaluated these quantities numerically for finite-thickness dipoles using the Numerical Electromagnetics Code [23], a method-of-moments based program. Each wire dipole was  $10^{-3}\lambda$  thick and divided into 25 computational segments. For each value of  $d$ ,  $g_n(\theta, \phi)$  was computed over  $11.25^\circ$  increments of azimuth and zenith and the results used to numerically approximate (33). Note that, in the absence of scattering among the antennas, each dipole could be considered omnidirectional,  $g_n(\frac{\pi}{2}, \phi) = 1$ , and (33) reduces to Clarke's [22] formula  $J_0(2\pi \frac{d}{\lambda} (m-n))$ , where  $J_0(x)$  is the zeroth-order Bessel function of the first kind.

The amplifier selected for this study is a low-cost SiGe, heterojunction bipolar transistor LNA [24] designed for use in the cellular band. In high-gain mode with  $R_{\text{bias}} = 510 \Omega$  and  $f_c = 900$  MHz, its impedance matrix and Rothe-Dahlke noise parameters are:

$$\begin{bmatrix} z_{11} & z_{12} \\ z_{21} & z_{22} \end{bmatrix} = \begin{bmatrix} 35.7 \angle -82.0^\circ & 2.74 \angle 91.8^\circ \\ 325 \angle 119^\circ & 46.1 \angle -23.3^\circ \end{bmatrix} \Omega$$

$$r_a = 9.45 \Omega, \quad g_a = 3.24 \text{ mS}, \quad z_{\text{cor}} = 35.3 \angle -114^\circ \Omega$$

This amplifier is nearly unilateral ( $z_{21} \gg z_{12}$ ) and the minimum noise figure is quite low (1.04 dB), ideal characteristics for front-end amplifiers. In practice the noise figure may

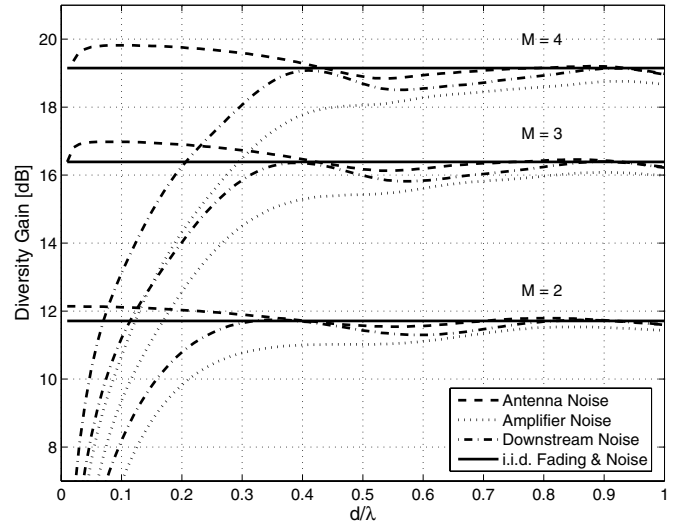


Fig. 4. Diversity gain for various noise sources and self-matching.

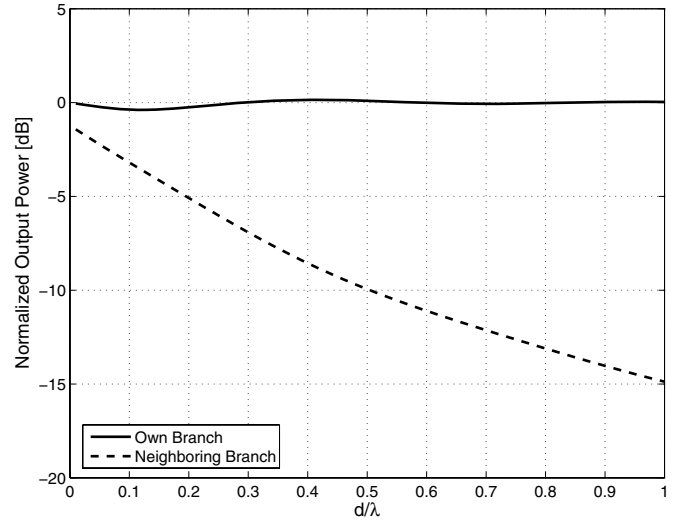


Fig. 6. Amplifier power coupling.

be slightly higher due to impedance mismatch and other implementation issues, but still low enough (a few dBs) that amplifier noise cannot be regarded as dominant over thermal antenna noise.

We calculate the downstream equivalent noise resistance  $r_d$  from a textbook example [17, pg. 654] in which the downstream components are a mixer with a 6 dB conversion loss and 7 dB noise figure and an intermediate-frequency amplifier with a 1.1 dB noise figure. The downstream noise figure is then  $\sim 7.6$  dB. Converting this to an equivalent noise resistance is not straightforward since the noise factor (6) depends on additional parameters. For the purpose of this example, we assume the downstream components take the composite form of a unilateral amplifier with a single input-referred noise source, and that the above noise figures were calculated with the standard  $Z_0 = 50 \Omega$  input impedance. The equivalent noise resistance is then

$$r_d = Z_0(F_{\text{down}} - 1) \approx 240 \Omega. \quad (34)$$

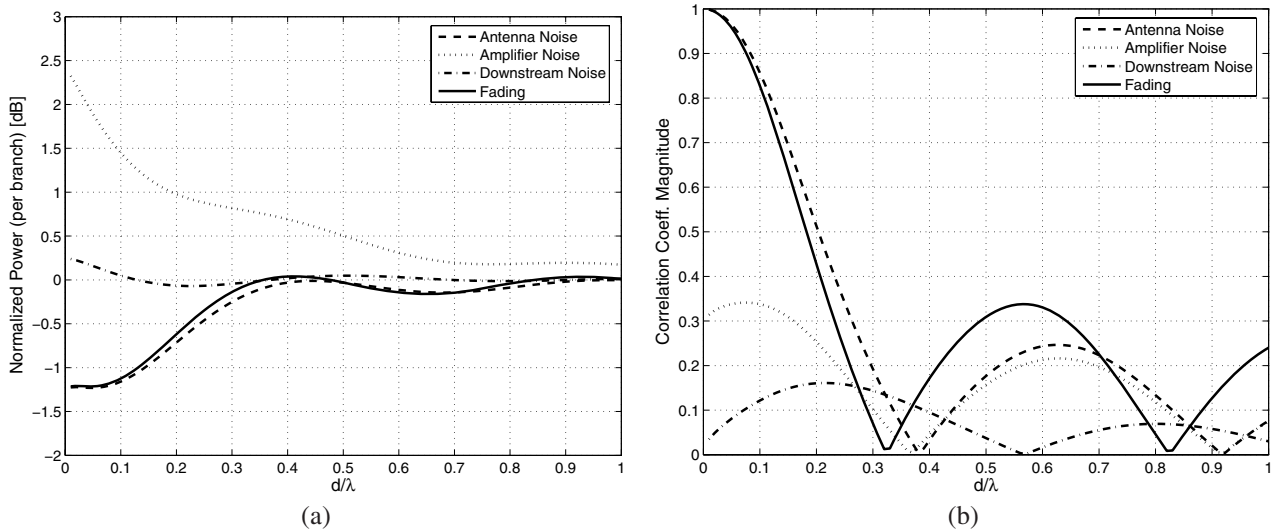


Fig. 5. Output signal and noise (a) power and (b) correlation in a dual-diversity system with self-matching.

### B. Multiport and Self Matching

We now evaluate outage for two matching networks considered in [9]. In *optimal multiport matching* for minimum noise figure, the network (31) is chosen so that  $\mathbf{Z}'_{\mathbf{A}} = z_{\text{opt}}\mathbf{I}$ , where  $z_{\text{opt}} = r_{\text{opt}} + jx_{\text{opt}}$  is the source impedance (8) that minimizes the amplifier noise factor  $F_{\text{amp}}$ . A lossless, reciprocal matching network that accomplishes this task is

$$\begin{bmatrix} \mathbf{Z}_{\mathbf{M}11} & \mathbf{Z}_{\mathbf{M}12} \\ \mathbf{Z}_{\mathbf{M}21} & \mathbf{Z}_{\mathbf{M}22} \end{bmatrix} = j \begin{bmatrix} -\mathbf{X}_{\mathbf{A}} & (r_{\text{opt}}\mathbf{R}_{\mathbf{A}})^{1/2} \\ (r_{\text{opt}}\mathbf{R}_{\mathbf{A}})^{1/2} & x_{\text{opt}}\mathbf{I} \end{bmatrix} \quad (35)$$

where  $\mathbf{X}_{\mathbf{A}} \triangleq \frac{1}{2j}(\mathbf{Z}_{\mathbf{A}} - \mathbf{Z}'_{\mathbf{A}})$ .

The matching network (35) may be difficult to realize in practice. A simpler, suboptimum strategy is to apply to each receive antenna the two-port matching network that achieves the minimum noise figure for that antenna in isolation. This is called *self matching* for minimum noise figure and is accomplished by the network

$$\begin{bmatrix} \mathbf{Z}_{\mathbf{M}11} & \mathbf{Z}_{\mathbf{M}12} \\ \mathbf{Z}_{\mathbf{M}21} & \mathbf{Z}_{\mathbf{M}22} \end{bmatrix} = j \begin{bmatrix} -x_{\mathbf{A}}\mathbf{I} & \sqrt{r_{\text{opt}}r_{\mathbf{A}}}\mathbf{I} \\ \sqrt{r_{\text{opt}}r_{\mathbf{A}}}\mathbf{I} & x_{\text{opt}}\mathbf{I} \end{bmatrix} \quad (36)$$

where  $z_{\mathbf{A}} = r_{\mathbf{A}} + jx_{\mathbf{A}}$  is the self-impedance of each antenna in isolation.

Diversity gains for both multiport and self matching are shown in Fig. 3, with the i.i.d. fading and noise case (24) included for reference. At close inter-element spacings there is a dramatic difference between the two matching networks – gain for self-matching drops sharply for small  $d$ , while multiport matching does not. For example, there is little benefit ( $< 1$  dB for  $M = 3, 4$ ) in using more than two self-matched antennas for a *fixed* receiver aperture of  $0.2\lambda$ , while there is apparently a significant benefit for multiport matching.

### C. Noise Sources

We now examine the impact of each noise source by considering antenna, amplifier, and downstream noise individually. For multiport matching  $\mathbf{Z}'_{\mathbf{A}} = z_{\text{opt}}\mathbf{I}$ , so from (32)

$$\Sigma = \sigma r_{\mathbf{A}}\mathbf{R}_{\mathbf{A}}^{-1/2}\Sigma_{\mathbf{h}}\mathbf{R}_{\mathbf{A}}^{-1/2}, \quad (37)$$

where  $\sigma$  is the SNR of a single-antenna system (10) with  $T_{\mathbf{A}} = T_0$  and  $z_{\mathbf{A}} = z_{\text{opt}}$ . Since diversity gain is unchanged by scalar multiples of  $\Sigma$ , the impact of each noise source is identical for multiport matching. For self-matching, however, there is a strong dependence on the relative strength of each noise source. This is illustrated in Fig. 4, where diversity gain curves are shown for systems in which each source is dominant. Note that noise from the amplifiers has the most detrimental affect, while antenna thermal noise appears to be more benign. The curves in Fig. 3, where all three noise sources are present, represent the combined effect of the curves in Fig. 4.

For  $M = 2$ , we can gain insight by examining how the power and correlation of each noise source varies with antenna spacing  $d$ . These parameters can be calculated from the matrices (25)-(27) with  $\mathbf{Z}_{\mathbf{A}}$  replaced by  $\mathbf{Z}'_{\mathbf{A}}$ . For example, the antenna noise power in each branch is  $P = [\Sigma_{\text{ant}}]_{11} = [\Sigma_{\text{ant}}]_{22}$ , and the correlation between the noise in each branch is  $\rho = [\Sigma_{\text{ant}}]_{12}/[\Sigma_{\text{ant}}]_{11}$ . In Fig. 5, we plot  $P$  and  $\rho$  for each noise source, and for the fading path gains (33). In this plot, each power is normalized by the corresponding power for  $M = 1$ . From Fig. 5(a), note that amplifier noise power increases as the antennas move closer. This explains the negative impact of amplifier noise in Fig. 4, and is caused by each antenna recapturing amplifier noise radiated from its neighbor. This is illustrated in Fig. 6, where the noise power an amplifier contributes to its own branch is compared to the power it contributes to the *other* branch. In Fig. 5(b) we see that both fading and antenna noise become highly correlated as the antennas move closer. Since correlated noise is generally desirable in communications, exploiting this correlation in our model mitigates the undesirable impact of fading correlation for small  $d$ . Finally, observe that downstream noise power is relatively constant and correlation low for most  $d$ , similar to white noise. Indeed, setting  $\Sigma_{\mathbf{n}} = \mathbf{I}$  and repeating the self-match simulations in Fig. 3 produced curves (not shown) almost indistinguishable from the downstream noise curves in Fig. 4. As discussed in Sec. V, this is due to the amplifier unilaterality that isolates downstream components from the coupled antennas. If the amplifier was perfectly unilateral

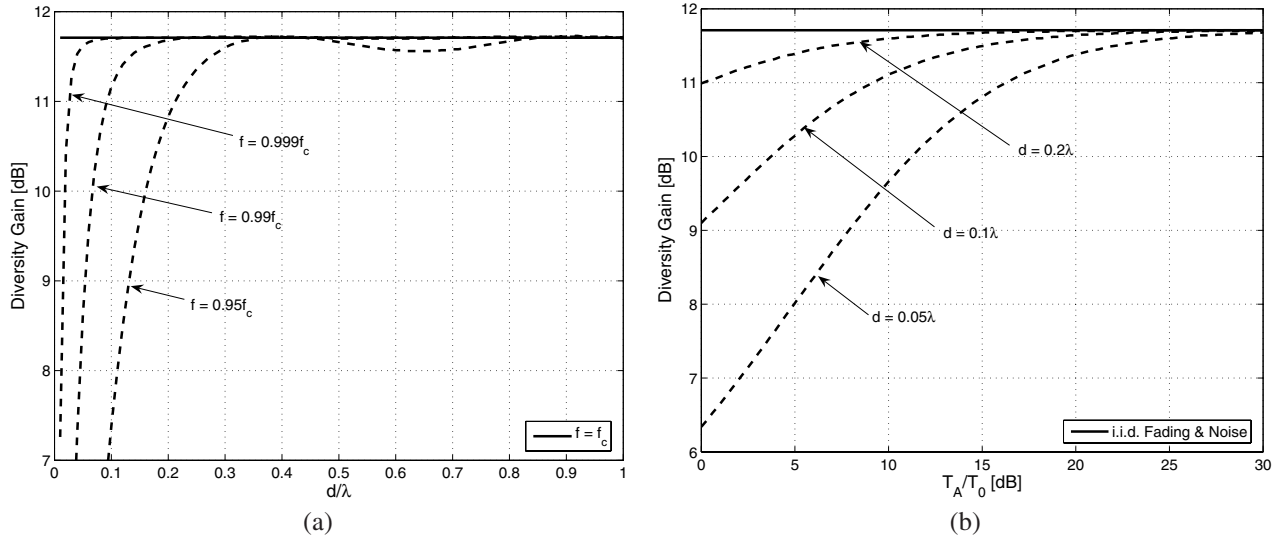


Fig. 7. Diversity gain with 3D fading. (a) Multiport matching at various multiples of the center frequency  $f_c$ . (b) Antenna noise of varying strength.

( $z_{12} = 0$ ), both downstream noise curves in Fig. 5 would be exactly zero at all spacings.

#### D. 3D Scattering

At the end of Section IV we mentioned that systems with proportional fading and noise correlation matrices have the same outage probability as a system with i.i.d. fading and noise. In this section we examine two cases of this phenomenon, both of which follow from a well-known result in electromagnetics that we briefly present below.

Consider operating the array in transmit mode by applying a current  $\mathbf{i} = [i_1 \cdots i_M]^T$  to its terminals. By superposition and reciprocity, the electric field at a large distance  $r$  from the array (i.e., in the radiation zone) is given by  $\hat{\theta} \frac{1}{r} e^{-j\frac{2\pi}{\lambda}r} \sum_n i_n g_n(\theta, \phi) e^{j\frac{2\pi}{\lambda}d(1-n)\sin\theta\cos\phi}$ , where  $\hat{\theta}$  is the unit vector oriented along the  $\theta$  direction. The array is lossless, so the real power delivered to the antennas must be equal to the radiated power:

$$\mathbf{i}^\dagger \mathbf{R}_A \mathbf{i} = \frac{1}{\eta_0} \int_0^{2\pi} \int_0^\pi \left| \sum_n i_n g_n(\theta, \phi) e^{j\frac{2\pi}{\lambda}d(1-n)\sin\theta\cos\phi} \right|^2 \sin\theta d\theta d\phi,$$

where  $\eta_0 \approx 120\pi \Omega$  is the impedance of free space. Since this holds for all  $\mathbf{i}$  we conclude that

$$[\mathbf{R}_A]_{nm} = \frac{1}{\eta_0} \int_0^{2\pi} \int_0^\pi g_n(\theta, \phi) g_m^*(\theta, \phi) e^{j\frac{2\pi}{\lambda}d(m-n)\sin\theta\cos\phi} \sin\theta d\theta d\phi. \quad (38)$$

This result is well-known in the antenna community (sometimes expressed in terms of scattering parameters, cf. [25]), and has been used in the context of communications to relate fading correlation and mutual impedances [26]. In particular, for a 3D scattering model in which the received electric field arrives from each direction with equal probability, i.e.,  $p(\theta, \phi) = \frac{1}{4\pi}$ , from (33) and (38) we see that  $\Sigma_{\mathbf{h}} = \frac{\eta_0}{4\pi} \mathbf{R}_A$ .

Here we are concerned with two consequences of this result observed in<sup>7</sup> [10],[11] that also hold for our model:

- 1) For 3D scattering and multiport matching (cf. Sec. VII-B), from (37) we see that<sup>8</sup>  $\Sigma = \frac{\sigma\eta_0}{4\pi} \mathbf{I}$ .
- 2) For 3D scattering and any lossless matching network, when antenna noise is dominant (i.e., we can zero  $r_a$ ,  $g_a$ , and  $r_d$  without appreciably changing  $\Sigma_{\mathbf{n}}$ ), from (32) we have

$$\Sigma = \frac{\mathcal{E}}{4kT_0B} \mathbf{M} \Sigma_{\mathbf{h}} \mathbf{R}_A^{-1} \mathbf{M}^{-1} = \frac{\mathcal{E}\eta_0}{16\pi kT_0B} \mathbf{I}, \quad (39)$$

where we observed  $\mathbf{R}'_A = \mathbf{M} \mathbf{R}_A \mathbf{M}^\dagger$  for lossless matching, cf. (31).

In both cases the diversity gain is identical to that of a system with i.i.d. fading and noise, regardless of inter-element spacing. This result is unsettling since it suggests that, at least in theory, one may realize unbounded performance improvements by packing an arbitrarily large number of antennas into a small space. However, we show below that for small  $d$  both observations are extremely sensitive to other system parameters.

Let us begin with observation 1). In this paper we have assumed a narrowband, frequency-flat system, so the array impedance and radiation pattern were computed at a single frequency  $f_c$  (the value of  $f_c$  is immaterial since the antenna parameters may be normalized by  $\lambda$ , e.g., we are using a  $\frac{\lambda}{2}$ -length dipole). To test whether these results are valid in a useable frequency band around  $f_c$ , we recalculated the transformed array impedance matrix  $\mathbf{Z}'_A$  and induced voltage  $\mathbf{v}'_o$  with the multiport matching tuned to  $f_c$  and the array parameters calculated at  $0.999f_c$ ,  $0.99f_c$ , and  $0.95f_c$ . The resulting diversity gain is shown in Fig. 7(a). Performance is equal to an i.i.d. fading and noise system at exactly  $f_c$ ,

<sup>7</sup>Recall that the receiver model in these references is a special case of Fig. 2 in which the amplifiers are unilateral with no input noise (see our discussion in Section V) and downstream noise is neglected.

<sup>8</sup>In Fig. 3, where 2D scattering is assumed, the multiport curves are quite close to the i.i.d. fading and noise curves. Here the dipole radiation pattern attenuates many of the AoAs in the support set of  $p(\theta, \phi)$  exclusive to 3D scattering.

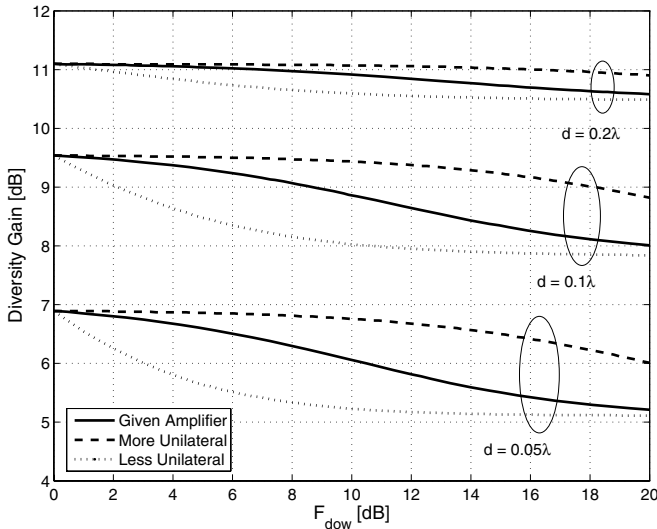


Fig. 8. Diversity gain as a function of downstream noise figure at various antenna spacings and amplifier unilaterality.

as predicted, but drops off dramatically from this frequency for small  $d$ . A similar conclusion is reached in [27] for a decoupling matching network optimized for maximum power transfer in a system with i.i.d. noise. As noted in [11], this sharp bandwidth reduction is an artifact of supergain behavior. The problems associated with superdirective arrays have been well-chronicled in the antenna design literature (cf., [14, pg. 345]) and their implications for MIMO are considered in [28].

Now consider observation 2). Since it is clear from (32) that  $\Sigma$  is non-diagonal when we include receiver noise (i.e.,  $r_a$ ,  $g_a$ , and  $r_d$  are nonzero), it is interesting to consider how large we must make the antenna temperature in order to approximate an i.i.d. system. To answer this question we re-evaluated the self-matching system in Sec. VII-B with 3D scattering and  $T_A \neq T_0$ . The resulting diversity gain is shown in Fig. 7(b) as a function of antenna temperature for several inter-element spacings. Note that for  $d = 0.2\lambda$ ,  $T_A$  only needs to be a few hundred Kelvin above standard temperature to approach the i.i.d. curve, but for  $d = 0.05\lambda$  this same result requires a tremendously large temperature. Such large temperatures are usually non-thermal in origin (cf., [17, Fig. 13.6]), e.g., from a strong source of Gaussian interference.

### E. Downstream Noise

As discussed in Sec. V, downstream noise becomes correlated by traversing the reverse signal path (output to input) of the amplifiers and coupling through the antennas. In this example we quantify how amplifier unilaterality and antenna mutual coupling alter the impact of downstream noise on the self-matching receiver of Sec. VII-B. We consider 3D scattering and set  $T_A = T_0$ .

In Fig. 8 we plot diversity gain as a function of downstream noise figure (34), parameterized by various degrees of amplifier unilaterality and inter-element spacings. To make the amplifier [24] more (less) unilateral we performed the transformation  $\{z_{12}, z_{21}\} \rightarrow \{\frac{1}{c}z_{12}, cz_{21}\}$  ( $\{z_{12}, z_{21}\} \rightarrow \{cz_{12}, \frac{1}{c}z_{21}\}$ ), where  $c = \sqrt{10}$ , which alters the relative strength of the

noise from the antennas (25) and amplifiers (26) while keeping the downstream noise (27) fixed. From this plot we see that when the antennas are strongly coupled and the amplifier is less unilateral, downstream noise has a significant impact on diversity gain, even for relatively low-noise devices (e.g.,  $F_{\text{dow}} \sim 3$  dB). For example, at  $d = 0.05\lambda$  increasing the downstream noise figure from 0 to 10 dB reduces diversity gain by almost 2 dB for the “less unilateral” amplifier, while there is little change in diversity gain for the “more unilateral” amplifier. On the other hand, at  $d = 0.2\lambda$  varying both the downstream noise figure and amplifier unilaterality yields negligible change in performance.

### F. Directional Fading and Sky Noise

In Fig. 7(b) we observed that large antenna temperatures were required to render receiver noise negligible. Such large temperatures are usually non-thermal in nature and arise from a strong source of Gaussian interference. In contrast to spherically isotropic thermal noise, interference is typically directional, so in this example we consider directional fading and sky noise.

Let us model directional fading by (33) with  $p(\theta, \phi) = \delta(\theta - \frac{\pi}{2})u(\phi)$ , where  $u(\phi)$  is uniform over  $(-\frac{\phi_s}{2}, \frac{\phi_s}{2})$  and  $\phi_s \in [0, 2\pi]$  is the *angular spread*. We may replace the thermal antenna noise model used throughout this paper with directional sky noise of the same form as (33) by taking  $\mathbf{n}_o \sim \mathcal{CN}(\mathbf{0}, \Sigma_o)$ , where the entries  $[\Sigma_o]_{nm}$  of the correlation matrix are given by

$$\frac{4kT_A B r_A}{\phi_s} \int_{-\phi_s/2}^{\phi_s/2} g_n(\pi/2, \phi) g_m^*(\pi/2, \phi) e^{j \frac{2\pi}{\lambda} d(m-n) \cos \phi} d\phi, \quad (40)$$

which is normalized so that the sky noise power of a single-antenna receiver is  $4kT_A B r_A$ . We continue with the self-matching receiver model, so the SNR matrix is given by (32) with the  $4kT_A B \mathbf{R}'_A$  term replaced by (40). For the purpose of this example we simply take  $T_A = T_0$ .

Diversity gain for various angular spreads of fading and sky noise are shown in Fig. 9(a). In the directional fading curve the sky noise is omnidirectional ( $\phi_s = 2\pi$ ), and the opposite applies for the directional sky noise curve. The correlation coefficient corresponding to various angular spreads is provided in Fig. 9(b) for reference. Note that directional fading is generally much more harmful than directional sky noise is beneficial. For example, reducing the angular spread of fading from  $360^\circ$  to  $45^\circ$  results in an almost 7 dB drop in diversity gain over the entire range of inter-element spacings, while reducing the sky noise angular spread by the same amount only improves performance by about 1 dB. This can be explained by observing that directional fading changes the entire signal correlation matrix in (32), whereas directional sky noise affects only the first term of the noise correlation (i.e., amplifier and downstream noise are unchanged). Of course, if antenna noise were dominant the benefit of directional sky noise would increase.

## VIII. CONCLUSION

A model for a compact diversity receiver was presented that articulates noise from the antennas, front-end amplifiers,

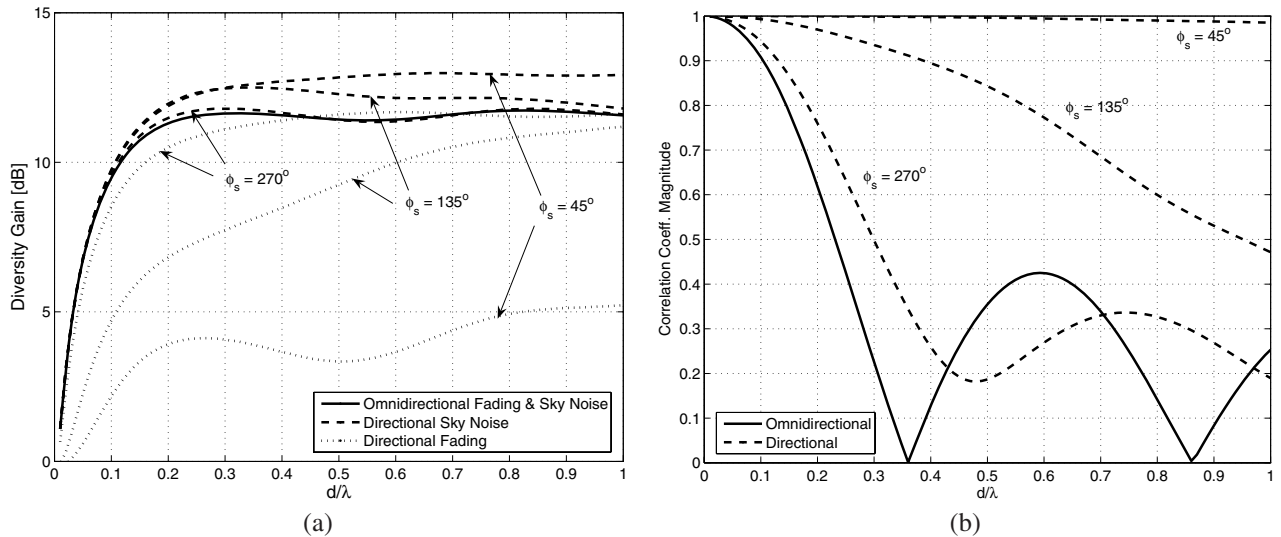


Fig. 9. (a) Diversity gain and (b) correlation for directional fading and sky noise with various angular spreads.

and downstream components. Using this model we showed that receiver noise is generally correlated between diversity branches, in contrast the common assumption of spatially white noise. In fact, our results suggest that, in the presence of strongly coupled antennas, some stringent assumptions on the dominant source of noise and receiver structure may be needed to justify a white noise model.

We considered several examples of receivers to illustrate the characteristics of different noise sources. These examples suggest that the sources behave in profoundly different ways:

- Thermal noise from the antennas has the least detrimental effect on diversity gain since it becomes highly correlated at close antenna spacings.
- Amplifier noise can reduce diversity gain more than any other noise source since it can spread through neighboring receiver chains as the antennas become strongly coupled.
- Noise generated downstream from the amplifiers is usually well isolated from the coupled antennas and thus behaves quite similar to spatially white noise. Its impact on diversity gain is between that of antenna and amplifier noise.

Multipoint matching may significantly alter the above conclusions since one may decouple the antennas, however, at close antenna separations this may result in supergain effects that sharply reduce the system bandwidth.

While the above results are specific to the examples considered, some of the insights learned from this study may apply more broadly. Specifically, a spatially white noise model may not be accurate, even if the noise sources in each branch are independent and uncoupled. Each noise source is observed by the combiner (or any post-detection processor) only after interacting with the coupled antennas, which acts to correlate both the signal and noise components in each diversity branch. This effect is more significant for noise sources closer to the antennas, and is dependent on the unilaterality of the front-end amplifiers. We conclude that, in compact multi-antenna receivers, the impact of various noise sources depends on

receiver parameters (e.g., front-end amplifier unilaterality) that are usually not considered in a standard single-antenna receiver noise budget. This is a consequence of the fact that both the power *and correlation* of each noise source are important. It is therefore vitally important to carefully identify different sources of noise, as they may have profoundly different effects on performance.

## REFERENCES

- [1] W. C. Y. Lee, "Mutual coupling effect on maximum-ratio diversity combiners and application to mobile radio," *IEEE Trans. Commun. Technol.*, vol. COM-18, pp. 779-791, Dec. 1970.
- [2] I. J. Gupta and A. A. Ksienski, "Effect of mutual coupling on the performance of adaptive arrays," *IEEE Trans. Antennas Propag.*, vol. AP-5, pp. 785-791, Sept. 1983.
- [3] T. S. Svantesson and A. Ranheim, "Mutual coupling effects on the capacity of multielement antenna systems," in *Proc. IEEE ICASSP*, 2001, pp. 2485-2488.
- [4] C. Waldschmidt, J. v. Hagen, and W. Wiesbeck, "Influence and modeling of mutual coupling in MIMO and diversity systems," in *Proc. IEEE AP-S Inter. Symp.*, 2002, pp. 190-193.
- [5] R. Janaswamy, "Effect of element mutual coupling on the capacity of fixed length linear arrays," *Antennas Wireless Propag. Lett.*, vol. 1, pp. 157-160, 2002.
- [6] B. Clerckx, D. Vanhoenacker-Janvier, C. Oestges, and L. Vandendorpe, "Mutual coupling effects on the channel capacity and the space-time processing of MIMO communication systems," in *Proc. IEEE ICC*, 2003, pp. 2638-2642.
- [7] J. W. Wallace and M. A. Jensen, "Mutual coupling in MIMO wireless systems: A rigorous network theory analysis," *IEEE Trans. Wireless Commun.*, vol. 3, pp. 1317-1325, July 2004.
- [8] X. Li and Z. Nie, "Mutual coupling effects on the performance of MIMO wireless channels," *IEEE Antennas Wireless Propag. Lett.*, vol. 3, pp. 344-347, 2004.
- [9] M. L. Morris and M. A. Jensen, "Improved network analysis of coupled antenna diversity performance," *IEEE Trans. Wireless Commun.*, vol. 4, pp. 1928-1934, July 2005.
- [10] M. J. Gans, "Channel capacity between antenna arrays – part I: Sky noise dominates," *IEEE Trans. Commun.*, vol. 54, pp. 1586-1592, Sept. 2006.
- [11] M. J. Gans, "Channel capacity between antenna arrays – part II: Amplifier noise dominates," *IEEE Trans. Commun.*, vol. 54, pp. 1983-1992, Nov. 2006.
- [12] S. M. Krusevac, R. A. Kennedy, and P. B. Rapajic, "Effect of signal and noise mutual coupling on MIMO channel capacity," *Wireless Personal Commun.*, vol. 40, pp. 317-328, Feb. 2007.
- [13] C. P. Domizioli, B. L. Hughes, K. G. Gard, and G. Lazzi, "Receive diversity revisited: correlation, coupling and noise," in *Proc. IEEE GlobeCom*, pp. 3601-3606, Nov. 2007.

- [14] C. A. Balanis, *Antenna Theory: Analysis and Design*, 3rd ed. NY: Wiley, 2005.
- [15] W. R. Bennett, *Electrical Noise*. NY: McGraw Hill, 1960.
- [16] R. Q. Twiss, "Nyquist's and Thevenin's theorems generalized for nonreciprocal linear networks," *J. Appl. Physics*, vol. 26, pp. 599-602, May 1955.
- [17] D. M. Pozar, *Microwave Engineering*, 3rd ed. NY: Wiley, 2005.
- [18] H. Rothe and W. Dahlke, "Theory of noisy fourpoles," in *Proc. IRE*, vol. 44, pp. 811-818, June 1956.
- [19] D. G. Brennan, "Linear diversity combining techniques," in *Proc. IRE*, vol. 47, pp. 1075-1102, June 1959.
- [20] R. A. Horn and C. R. Johnson, *Matrix Analysis*. NY: Cambridge, 1985.
- [21] H. A. Haus and R. B. Adler, *Circuit Theory of Linear Noisy Networks*. NY: Wiley, 1959.
- [22] R. H. Clarke, "A statistical theory of mobile-radio reception," *Bell Syst. Tech. J.*, vol. 47, pg 957-1000, July 1968.
- [23] G. J. Burke and A. J. Poggio, "Numerical Electromagnetics Code (NEC) – Method of moments," Tech. Doc. 11, Naval Ocean Systems Center, San Diego, CA, Jan. 1981.
- [24] Maxim 2642/2643 LNAs. Data sheet [Online]. Available: <http://datasheets.maxim-ic.com/en/ds/MAX2642-MAX2643.pdf>
- [25] S. Stein, "On cross coupling in multiple-beam antennas," *IRE Trans. Antennas Propag.*, vol. 10, pp. 548-557, Sept. 1962.
- [26] R. G. Vaughan and J. B. Anderson, "Antenna diversity in mobile communications," *IEEE Trans. Veh. Technol.*, vol. 36, pp. 149-172, Nov. 1987.
- [27] B. K. Lau, J. B. Anderson, G. Kristensson, and A. F. Molisch, "Impact of matching network on bandwidth of compact antenna arrays," *IEEE Trans. Antennas Propag.*, vol. 54, pp. 3225-3238, Nov. 2006.
- [28] M. L. Morris, M. A. Jensen, and J. W. Wallace, "Superdirectivity in MIMO systems," *IEEE Trans. Antennas Propag.*, vol. 53, pp. 2850-2857, Sept. 2005.



**Carlo Domizioli** (S'03-M'09) was born in Luton, England, on Nov. 7, 1980. He received the B.S. degree in electrical engineering from Tennessee Technological University, Cookeville, in May 2005, and the Ph.D. degree in electrical engineering from North Carolina State University, Raleigh, in Dec. 2009. He is currently a communication systems engineer for Northrop Grumman Information Systems in Fairfax, VA.



**Brian Hughes** (S'84-M'85) was born in Baltimore, MD, on July 16, 1958. In 1980, he received the B.A. degree in mathematics from the University of Maryland, Baltimore County. He received the M.A. degree in applied mathematics as well as the Ph.D. degree in electrical engineering from the University of Maryland, College Park, in 1983 and 1985, respectively.

From 1980 to 1983, he worked as a mathematician at the NASA Goddard Space Flight Center in Greenbelt, MD. From 1983 to 1985, he was a Fellow with the Information Technology Division of the Naval Research Laboratory in Washington, DC. From 1985 to 1997, he served as Assistant and then Associate Professor of Electrical and Computer Engineering at The Johns Hopkins University in Baltimore, MD. In 1997, he joined the faculty of North Carolina State University in Raleigh, where he is currently Professor of Electrical and Computer Engineering. His research interests include communication theory, information theory, and communication networks.

Dr. Hughes has served as Associate Editor for Detection of the IEEE Transactions on Information Theory, Editor for Theory and Systems of IEEE Transactions on Communications, and as Guest Editor for two special issues of IEEE Transactions on Signal Processing. He has also co-chaired the 2008 Globecom Wireless Communications Symposium, the 2004 Globecom Communication Theory Symposium, as well as the 1987 and 1995 Conferences on Information Sciences and Systems. He has also served on the program committees of numerous international conferences, including the IEEE Global Communications Conference, IEEE International Communications Conference, IEEE International Symposium on Information Theory, and the IEEE Wireless Communications and Networking Conference.



**Kevin G. Gard** (S'92-M'95) received the B.S. and M.S. degrees in electrical engineering from North Carolina State University, Raleigh, in 1994 and 1995, respectively, and the Ph.D. degree in electrical engineering from the University of California at San Diego, La Jolla, in 2003. He is currently a hardware design engineer at Ericsson Mobile Platforms designing CMOS front-end circuits for GSM, EDGE and WCDMA transceivers. From 2004 to 2008 he was the William J. Pratt Assistant Professor with the Electrical and Computer Engineering Department at North Carolina State University. From 1996 to 2003, he was with Qualcomm Inc., San Diego, CA, where he was a Staff Engineer and Manager responsible for the design and development of RF integrated circuits (RFICs) for code-division multiple-access (CDMA) wireless products. His research interests are in the areas of novel integrated circuit solutions for wireless transceivers and analysis of nonlinear microwave circuits with digitally modulated signals. He has authored or coauthored over 60 papers related to RF/analog integrated circuit design and analysis of nonlinear circuits. Dr. Gard is a member of the IEEE Microwave Theory and Techniques Society (IEEE MTT-S) and IEEE Solid-State Circuits Society. He is a member of Eta Kappa Nu and Tau Beta Pi. In 2007, He was secretary of the IEEE MTT-S Administrative Committee (AdCom) in 2007.



**Gianluca Lazzi** (S'94-M'95-SM'99-F'08) received the Dr.Eng. degree in electronics from the University of Rome "LaSapienza," Rome, Italy, in 1994, and the Ph.D. degree in electrical engineering from the University of Utah, Salt Lake City, in 1998. He is currently a USTAR Professor and Department Chair at the Department of Electrical and Computer Engineering, The University of Utah, Salt Lake City, UT. Since 2007, he was a Professor with the Department of Electrical and Computer Engineering, North Carolina State University (NCSU), where he

was an Assistant Professor from 1999 to 2003 and an Associate Professor from 2003 to 2006.

He has been a Visiting Researcher with the Italian National Board for New Technologies, Energy, and Environment (ENEA) (1994), a Visiting Researcher with the University of Rome "La Sapienza" (1994-1995), and a Research Associate (1995-1998) and Research Assistant Professor (1998-1999) with the University of Utah. He has authored or coauthored over 100 international journal papers or conference presentations on implantable devices, medical applications of electromagnetic fields, antenna design, FDTD modeling, dosimetry, and bioelectromagnetics. Dr. Lazzi was the Chair of Commission K (Electromagnetics in Biology and Medicine) of the U.S. National Committee of the International Union of Radio Science (URSI) (2006-2008). He was the recipient of the 1996 "Curtis Carl Johnson Memorial Award" for the best student paper presented at the 18th Annual Technical Meeting of the Bioelectromagnetics Society (BEMS), a 1996 International Union of Radio Science (URSI) Young Scientist Award, a 2001 Whitaker Foundation Biomedical Engineering Grant for Young Investigators, a 2001 National Science Foundation (NSF) CAREER Award, a 2003 NCSU Outstanding Teacher Award, the 2003 NCSU Alumni Outstanding Teacher Award, the 2003 ALCOA Foundation Engineering Research Award, the 2006 H.A. Wheeler award from the IEEE Antennas and Propagation Society for the best application paper published in IEEE TRANSACTIONS ON ANTENNAS AND PROPAGATION in 2005, and a 2008 best paper award at the IEEE conference "GlobeCom," and the 2009 ALCOA Foundation Distinguished Engineering Research Award. He has been an Associate Editor for the IEEE ANTENNAS AND WIRELESS PROPAGATION LETTERS (2001-2007) and served as a Guest Editor for the Special Issue on Biological Effects and Medical Applications of RF/Microwaves of the IEEE TRANSACTIONS ON MICROWAVE THEORY AND TECHNIQUES in 2004. Since January 2008, he has been the Editor-in-Chief of IEEE ANTENNAS AND WIRELESS PROPAGATION LETTERS.